Progress in Nuclear Energy 164 (2023) 104854

Contents lists available at ScienceDirect

Progress in Nuclear Energy

journal homepage: www.elsevier.com/locate/pnucene

Detail CFD simulation of the integrated reactor pressure vessel of SMART

Michael Böttcher, Victor Sanchez-Espinoza *

Karlsruhe Institute of Technology, Institute for Neutron Physics and Reactor Technology, Hermann-von-Helmholtz-Platz 1, D-76344, Eggenstein-Leopoldshafen, Germany

ARTICLE INFO

Keywords:
CFD
SMART
SMR
Thermal hydraulic analysis
TRACE

ABSTRACT

This paper presents a detailed analysis of the full Reactor Pressure Vessel (RPV) of SMART with ANSYS CFX 20.2. SMART is a water-cooled SMR designed by KAERI for an operation with forced convection. The thermal power of SMART amounts to 330 MW_{th}. In the integrated SMR-concept, the main primary loop components such as the helical steam generators, pressurizer and canned pumps are located inside the RPV. The CFD model uses a concept of full geometrical detail resolution with partial boundary inflation of the mesh and porous media modelling with sources for momentum and energy for components like the core, pumps and steam generators. The detailed results obtained with a steady-state RANS simulation using ANSYS CFX 20.2 are very promising as the comparison of selected core parameters of the CFD-simulation with the ones of the system thermal hydraulic code TRACE have shown.

1. Introduction

In the frame of the European McSAFER project (Sanchez-Espinoza et al., 2021), experimental and numerical investigations for the safety evaluation of water-cooled SMR are performed, where the multiscale and multiphysics methods play a central role. Hence, new calculation approaches are under development aimed at multiscale coupling of system thermal hydraulic codes with CFD and subchannel codes to improve the prediction accuracy of the three-dimensional thermal hydraulic phenomena within integrated RPV of SMRs. For this purpose, the development of CFD-models of integrated RPV including the core or parts of it, e.g. the downcomer and lower plenum are required. This paper presents the developed RPV-model of SMART (**S**ystem integrated **M**odular **A**dvanced **R**eac**T**ors) for ANSYS CFX20.2. SMART is a small pressurized water reactor with a thermal power up to 300 MW (100 MW electric) being developed by KAERI. SMART reactors are applicable for electricity production as well as to provide heat for desalination purposes with output to meet the demands for a smaller city with a population of 100000. A specific feature of the design is the arrangement of all primary components such as steam generators (SG's), the reactor coolant pumps, the pressurizer, and core structures inside the vessel. Fig. 1 shows the component arrangement. The inner diameter of the vessel is about 5.3 m, while the inner height is 15.5 m. The vessel contains four canned pumps in horizontal arrangement and eight steam generators (SG's). In the right part from Fig. 1, the main flow path is illustrated. The coolant leaves the SG's downwards and enters into the flow mixer. It leaves the mixer in radial direction towards the inner vessel wall (blue small arrows) and enters the lower plenum. To achieve homogeneous mixing on the way to the core inlet, the coolant has to penetrate through a flow distribution skirt, which has the shape of a perforated cylinder. Then the coolant enters the core - indicated by red color-, which has in its active part a length of 2 m. Above this region, control rod guide tube structures are visible. Having passed the active core region, the coolant penetrates into an annular gap, which is formed by an outer cylindrical wall – a barrier against the vessel volume containing the steam generators- and a perforated inner wall. In its upper part towards the location of the pumps, the gap has a conical shape with increasing cross section. The pumps supply the coolant towards the upper inlet of steam generators (SG's) with a spiral-type rod arrangement for heat exchange with superheated steam on the secondary site. Previous CFD work by Bae, Kim and Park (Bae et al., 2013) and by Kim et al. (2015) considered parts of the vessel such as the mixing in the lower part located around the core. They presented a model for the flow mixer in detail resolution and distribution skirt as a porous region where the inlet is located below the SG exit and the outlet below the core entrance. Mingjun Wang et al. (2020a) investigated the lower plenum of a PWR with different type of internal structures by a full resolving CFD model. For all types they found a non-homogeneous mass flow distribution for the assemblies at the core inlet with a maximum for central assemblies.

Lianfa Wang et al. (2020b) performed a similar investigation for the upper plenum of a VVER1000 reactor. Different type of perforated

* Corresponding author.
E-mail address: victor.sanchez@kit.edu (V. Sanchez-Espinoza).

https://doi.org/10.1016/j.pnucene.2023.104854
Received 3 February 2023; Received in revised form 1 August 2023; Accepted 11 August 2023
Available online 23 August 2023

barrels were investigated. At the hot legs the most homogeneous temperature and flow distribution was obtained by a combination of several perforated barrels similar as installed in presently operating VVER systems. M.Wang, Manera, Petrov et al. (Wang et al., 2020c) investigated the design of a helical coiled heat exchanger used as PDHS (Passive Decay Heat removal System) in a lightwater reactor by detailed CFD and RELAP5 system tool simulations. 8 heat exchangers in similar design are included in SMART vessel. They concluded, that in case of station blackout 3 systems were sufficient to remove the decay heat of the core. An overview of the present status of CFD applications and future directions in PWR thermal hydraulic studies is given in the work of M. Wang et al. (2021). The trend is to generate CFD models for vessels with resolution of all details except the core, which still requires porous media modelling. Furthermore, more and more coupling between various software systems with different modelling concepts at different scales is in focus of research.

The motivation of this work was the development of a full detail vessel model with consideration of all components in full spatial resolution or by a porous media approach. Such a model can be used later on to investigate the thermal hydraulic behavior of SMART under asymmetric transient conditions such as in case of the failure of a pump or of a steam generator. The authors build on the previous experience developing detailed CFD-models of a VVER1000 pressure vessel including all primary loop components by Böttcher and Krüßmann (2010).

In Chapter 2, the modeling of the SMART reactor using the ANSYS CFX code and TRACE is described with special emphasis on the description of the CFD-models. The discussion of selected results obtained with ANSYS CFX and a comparison of the CFD-results with the ones of the system code TRACE is extensively presented in Chapter 3. Finally, a summary and outlook is provided in Chapter 4.

2. Description of the CFD and system thermal hydraulic models

The very first challenge in this research was the generation of a CAD based geometry of SMART RPV. Not all necessary data is available in literature. As consequence, several dimensions were estimated or technical details were added being necessary for structural integrity or improved coolant mixing to minimize temperature gradients or to obtain homogeneous flow distribution. The second challenge was to keep the resulting cell number in a reasonable range because of limited computational resources and for saving calculation time. This means, that for several parts an implementation as porous medium was mandatory such as the SG's and the core. The pressure losses were implemented as volumetric momentum sinks. The solver – ANSYS CFX 20.2- allows in porous media regions the treatment of a fluid and solid phase with a specification of heat transfer conditions between the two phases. For the SG's the solid part was considered as Inconel 690 and a heat transfer correlation for spiral type heat exchanger was used. By

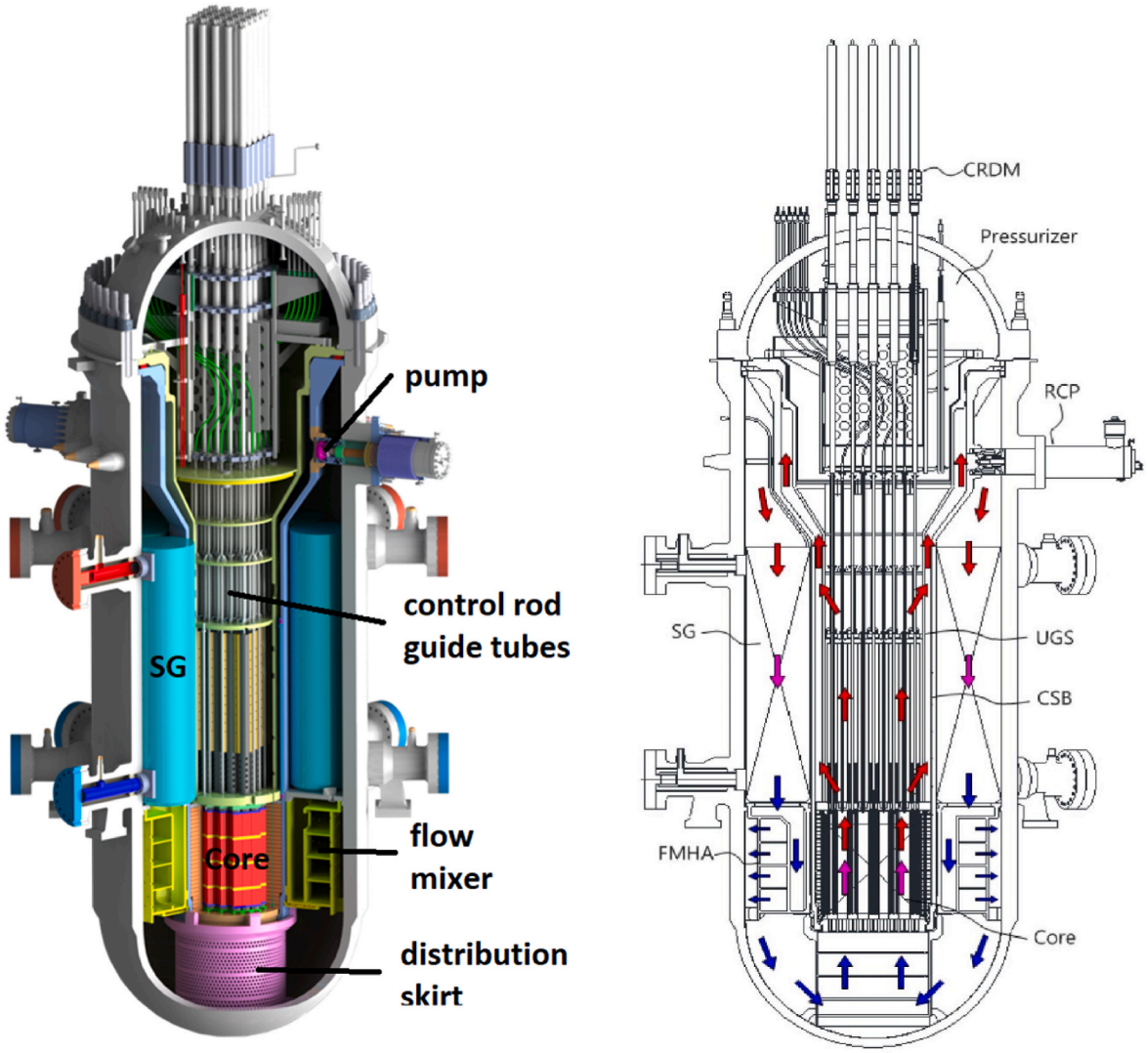

Fig. 1. Smart vessel layout and flow path visualization, see Choi (Choi, 2014).

specifying a heat transfer correlation for the heat transfer between Inconel and the steam phase on the secondary side it was also possible to calculate – of course in a simplified way-local steam temperatures. A similar approach was performed for the core.

The solid phase was considered as Zircaloy – the outer cladding material of the fuel rods. Then a heat transfer correlation considering the fuel rod arrangement was implemented and allowed to calculate a fuel rod outer surface temperature. By assuming a cladding thickness, a gap conductance between inner rod surface and fuel pellet, a pellet diameter and a pellet conductivity it was possible to calculate the maximum fuel temperature in the center of the fuel rods by assuming only radial heat transfer. With these model extensions it was possible to calculate maximum fuel temperatures, cladding temperatures and steam temperatures on the secondary side and to compare them with results from previously performed TRACE simulations. The computational grid was generated by meshing software from Pointwise (www.pointwise.com). The entire mesh contains about 49.8 mio cells. The core was constructed by full structured hexahedra, while for the other regions unstructured meshing was preferred. In order to save cells, boundary layer inflation was used only in regions with large velocity gradients and sensitivity for numerical stability, such as the vertical annular gap connecting the core outlet and the pump inlets and the inner vessel wall in the vicinity of the pumps. The spacing of the mesh varies between 1 mm for the wall closest layer thickness of inflated boundaries close to the pumps and 50 mm in the center of the SG's. It has to be menshioned that solid regions were not considered because of low thermal heat capacity compared with water and the low importance of conjugate heat transfer compared with heat transfer at forced convection conditions. Fig. 2 shows the mesh in the lower plenum with the flow distribution skirt with full resolution of all perforations. For a more realistic design in terms of mechanical stability, core support columns were implemented, which could not be found in present available publications about the Smart facility.

Also the space between core support plate and the core inlet was filled with nozzle structures in order to avoid local separation zones. Furthermore, the shape of the inner vessel wall in the lower plenum at the bottom was designed compatible with that of a VVER1000 vessel (see Kolev et al. (2006)). The red color indicates the active core region, while the blue color designates the core bypass channel.

In Fig. 3 the mesh in the upper plenum is shown. Again, some details were added or dimensions estimated that could not be found in publications but were necessary for the model design such as several perforation holes (top and bottom plates of the SG's etc.) and the wall inclination angles in the conical region of the previously discussed annular gap just below the pump inlets.

2.1. The pump model

One of the most crucial part mainly for the numerical stability was the design and meshing of the four horizontally installed pumps shown by Fig. 4. No pump impellers were modelled. Only the central pump axis was meshed. The intention was to generate a simplified configuration that was able to deviate the flow momentum direction in a similar way like the real pump without generating numerical instabilities. The flow through the created labyrinth is similar to that of a real pump, which is sucking fluid in direction of the pump axis and supplying into radial direction of its axis. Between the meander type channels, a limited mass transfer (small white arrows in Fig. 4) was allowed that fills up possible flow separation regions and stabilizes the main flow (red arrows). Furthermore, the mass flow through the pumps was achieved by setting

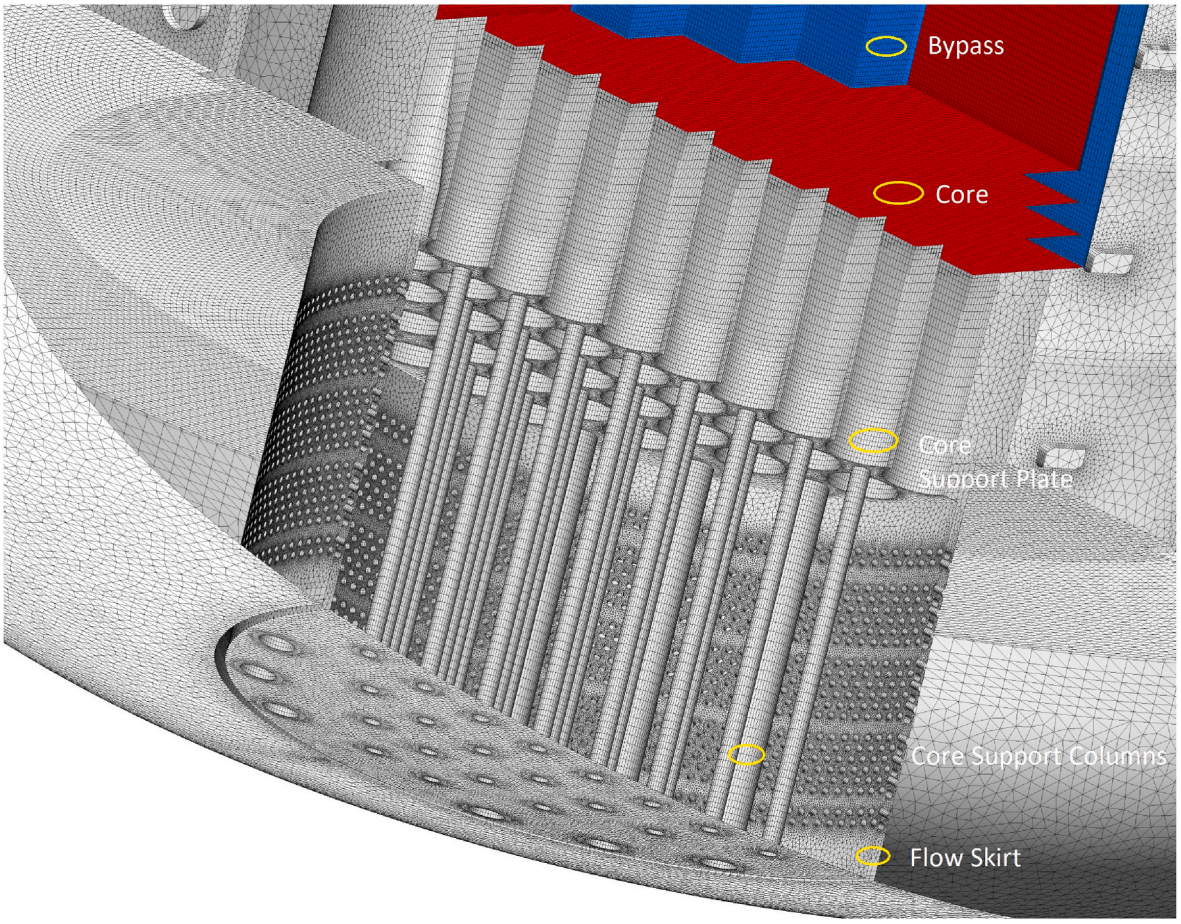

Fig. 2. Mesh in the lower plenum.

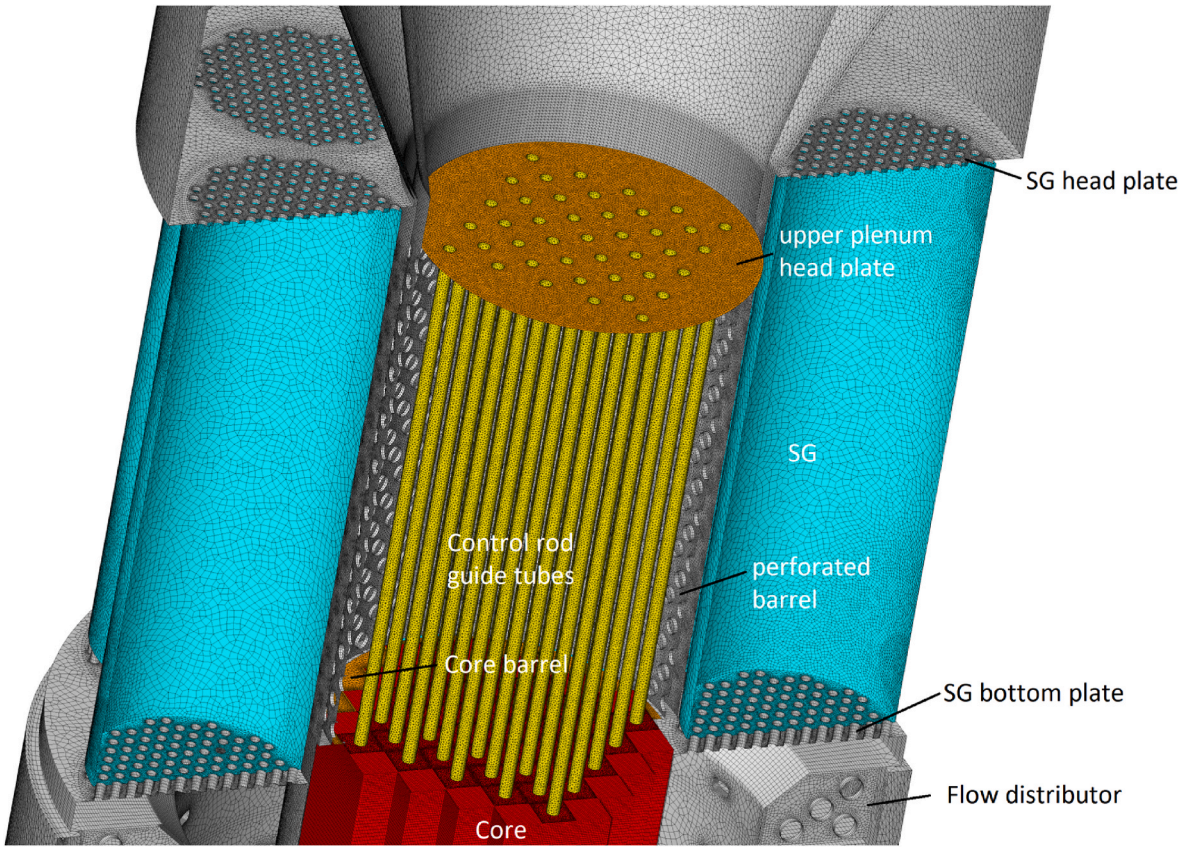

Fig. 3. The mesh in the upper plenum.

a mass flow boundary condition at the interface between pump inlet and the inner flow domain, designated as "int" within Fig. 4. In order to obtain a homogeneous flow distribution (and to stabilize the simulation) at the pump outlet a pressure loss coefficient (5000 m^{-1}) inside the pump domains was specified.

2.2. The core model

The SMART core is designed for a production of 330 MW_{th} and contains 57 fuel assemblies. Each assembly carries a 17 × 17 matrix of ceramic UO_2 fuel pins with an active length of 2 m. A more detailed description is given by IAEA (IAEA, 2005) and Horelik et al. (2013). Fig. 5 presents the total power of each assembly and the axial power distribution. Assemblies in central position generate the highest power, while in the outer positions the generated power decreases to about one third of the maximum. The total assembly powers were implemented in the CFD model as volumetric source terms with axial dependency given by averaged axial power factors as shown in Fig. 5. The core model is surrounded by four bypass channels as previously mentioned. They were designed for carrying 4% of the total mass flow entering the core. For numerical stability, the bypass channels were also treated as porous media with the same properties as the core but without volumetric heat deposition. It has to be mentioned that the core pressure loss was considered in terms of a uniform quadratic resistance coefficient. As consequence, the pressure loss is nearly constant in axial direction and does not consider any spacer locations.

With some extensions of the CFD model it was possible to calculate cladding and maximum fuel temperatures for a comparison with TRACE results. They were based on average assembly parameters given by Table 1, see also Marin (Mateo Marin, 2017). Furthermore, for the helium filled annular gap between pellet and cladding a heat transfer coefficient of 6300 W/m^2 K was assumed. The cladding material was considered as Zircaloy with a constant conductivity of 21.5 W/m K and fuel as UO_2 with a thermal conductivity similar with the UO_2 legacy model implemented in TRACE. The heat transfer between coolant and cladding surface was calculated by using a correlation for the Nusselt number by Gnielinski (1976):

$$Nu_{turb} = \frac{\left(\frac{f}{2}\right)(Re - 1000) \times Pr}{1 + 12.7\left(\frac{f}{2}\right)^{0.5}\left(Pr^{\frac{2}{3}} - 1\right)} \tag{1}$$

where f is a friction factor using smooth tube formula by Filonenko (1954):

$$f = [1.58 \times 1n(Re) - 3.28]^{-2} \tag{2}$$

with a validity range of $2300 \leq Re \leq 5 \times 10^6$ and $0.5 \leq Pr \leq 2000$.

2.3. The steam generator model

The Smart vessel contains 8 helical coiled steam generator units with basic geometrical parameters and operation conditions presented by Fig. 6. In the CFD model the SG's are modelled as cylindrical porous media regions with perforated head and bottom plates as shown by Fig. 3. The pressure loss is handled similar as in the core region by using a constant loss coefficient. The solid phase of the SG porous media zones is considered as Inconel 690. Between (primary) liquid and solid phase a heat transfer coefficient was specified, which finally allows a simplified calculation of SG rod surface temperatures:

$$\alpha = \frac{Q}{T_{coolant} - T_{pipe}} = Nu\,\frac{D_{hyd}}{\lambda_{coolant}} \tag{3}$$

where Q is the heat flux, D_{hyd} the hydraulic diameter, $\lambda_{coolant}$ the thermal conductivity and T_{pipe} the rod surface temperature. In the CFD model Q

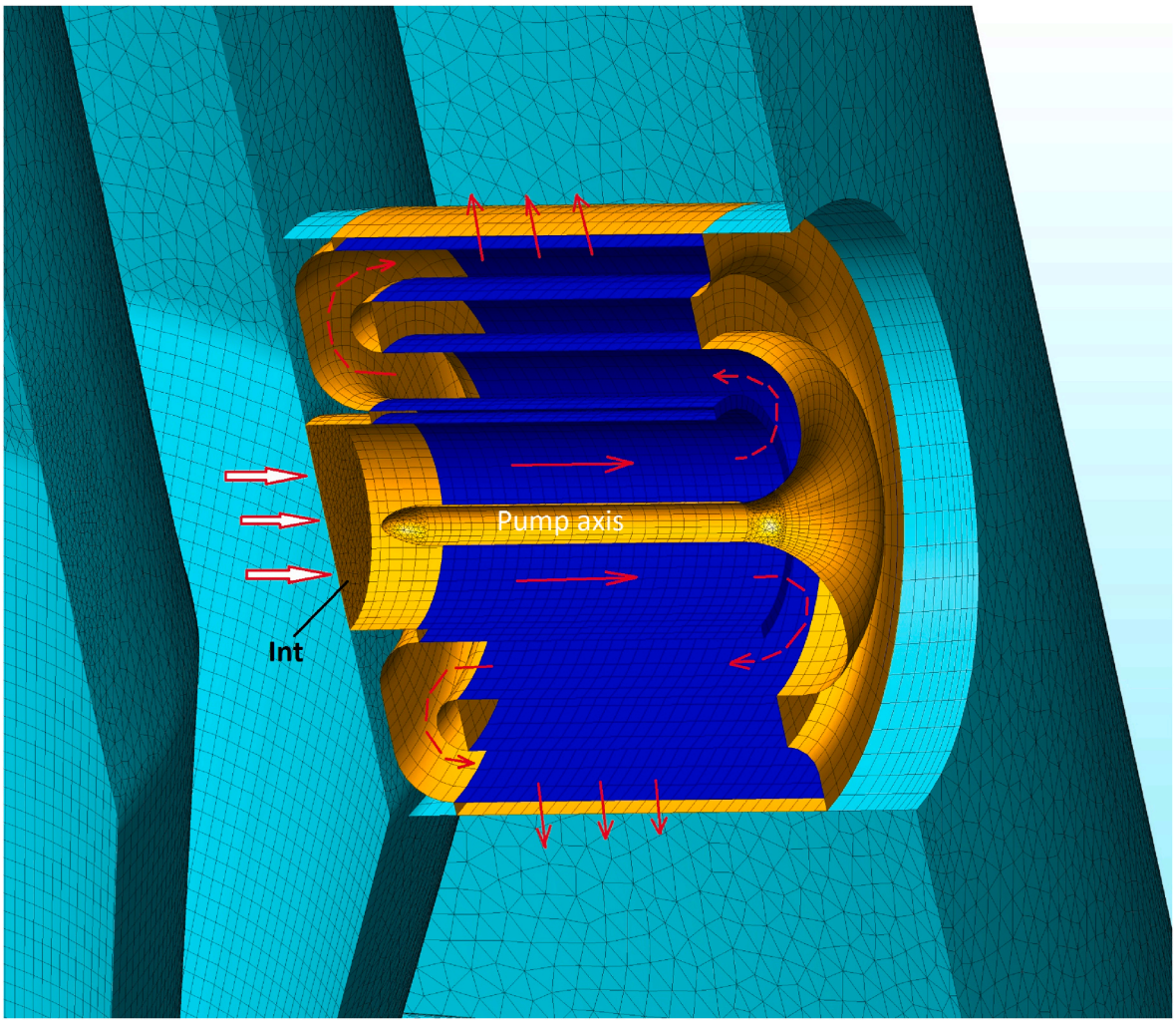

Fig. 4. Mesh detail of the pump.

is assumed as spatially constant and calculated as the ratio of Qs (see Fig. 6) and the total SG rod surface area.

For the Nusselt number of the primary side of the helical coiled SG pipes a correlation proposed by Kim and El-Genk (1988) is used:

$$Nu = C \bullet Re^{B} \bullet Pr^{D} \bullet \left(\frac{Pr}{Pr_w}\right)^{0.25} \quad (4)$$

where *Pr* is the Prandtl number in the bulk and Pr_w is the Prandtl number at wall. Eq. (4) – also used by TRACE - is a correlation for staggered cross flow with Re dependent constants presented by Table 2:

P is the pitch and D the pipe diameter, while T is indicating the transversal direction and L the longitudinal direction, see Trace manual (TRACE 5, 2013).

Where d_i is the SG pipe diameter and D_{hx} is the helical coil diameter. In this simulation values of 0.017 m and 0.7 m are used.

For the calculation of material properties the temperature has to be specified at a boundary or by specific temperature conditions at selected model regions. Therefore, the SG's heat removal is implemented as temperature dependent. At steady state conditions each steam generator removes 1/8 of the total core power of 330 MW, where the average SG temperature differences between inlet and outlet are corresponding with the average temperature heat up of the core. The heat sink for each SG is implemented as follows:

$$Q_{SG,i} = -\frac{1}{8} Q_{core} \frac{T_{SGin,i} - T_{core,in}}{T_{core,out} - T_{core,in}} \quad (5)$$

where $T_{SGin,i}$ is the average inlet temperature of steamgenerator i, $T_{core,in}$ and $T_{core,out}$ the average core inlet and outlet temperatures (569.15 K and 596.15 K).

2.3.1. Set-up of the CFD-models

The simulations were performed as steady state RANS (Reynolds Averaged Navier Stokes) single phase flow with temperature and pressure dependent water properties by using IAPWS (International Association for the Properties of Water and Steam) tables. The solid component property of SG's (Inconel 690) was implemented as temperature dependent, while for the porous core model the solid component was considered as Zircaloy with a constant thermal conductivity (21.5 W/m K). For the calculation of fuel temperatures the thermal conductivity of UO_2 was considered as temperature dependent similar with the UO_2 fuel legacy model in TRACE 5.0. Turbulence was implemented in terms of the SST (**S**hear **S**tress **T**ransport) model by Menter (1993). For stabilization of the solution a 1st order upwind scheme was applied.

As convergence criteria the standard values of 10^{-4} for normalized residuals and 10^{-2} as conservation target for global balances were applied. For the residuals, only values of $4*10^{-4}$ could be obtained. Temperature fluctuations at monitor points above the core up to 0.5 K (at 27 K average heat up by core passing) and small velocity fluctuations of 0.025 m/s close to the pumps (at an average velocity close to 9 m/s) indicated steady state conditions with a remaining transient background.

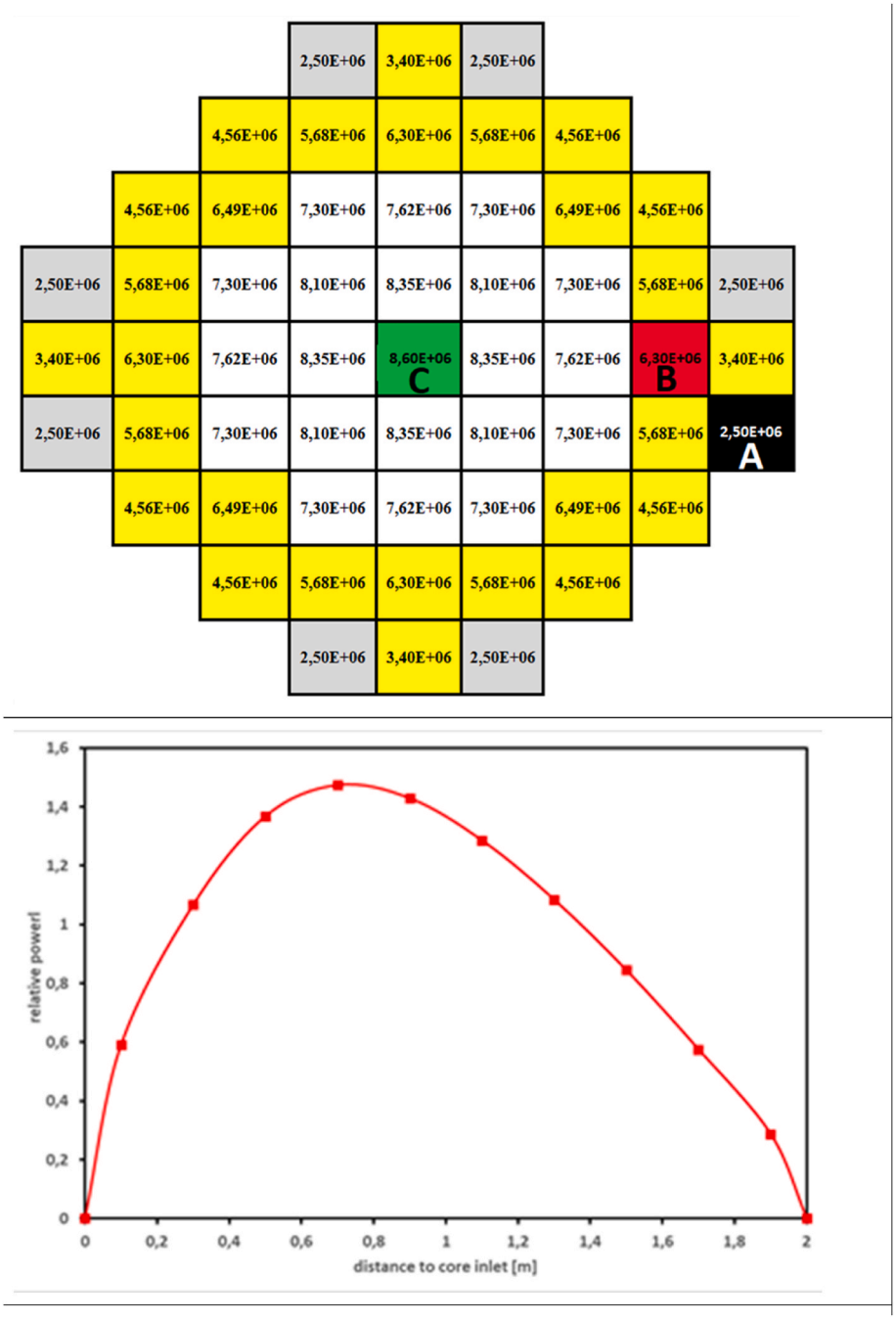

Fig. 5. Assembly power [W] (upper pos.) and core averaged axial power profile (lower pos.) (Choi, 2014).

Table 1
Fuel assembly parameters.

Assembly pitch	215.04 mm
Fuel rod diameter	9.14 mm
Pellet diameter	7.84 mm
Fuel rod array	17 × 17, square
rod pitch distance	12.6 mm
P/D	1.378

2.4. Short description of the TRACE model

The TRACE model of the SMART plant consists of the following parts:

- Core model consists of a Cartesian Vessel model,
- Integrated Reactor Pressure Vessel (RPV) represented by a Cylindrical Vessel, that includes components such as the pressurizer, the eight helical steam generators (SGs), pumps, and the flow mixing devices located around the core,
- In addition, the model contains the steam and feedwater lines, valves, the containment and the passive residual heat removal systems (PRHRS).

In the following subchapters, selected SMART-modelling issues are

Number of tubes	375
Tubes outer ⌀	17 mm
Tubes inner ⌀	12 mm
Tubes length	25.6 m
Coil average ⌀	906 mm
Tubes surface	500 m^2
Volume	8 m^3
Cassette height	6.4 m
Cassette outer ⌀	1.35 m
Tubes angle	8.41°
Radial pitch	22.5 mm
Axial pitch	20 mm
T1	596.2 K
T0	568.9 K
Qs	41 MW

Fig. 6. The helical coiled steam generator, see Choi (Choi, 2014) (left) and the main dimensions (right).

Table 2
Correlation constants for staggered cross flow.

Reynolds number	B	C	D
$1 \leq Re < 500$	0.4	1.04	0.36
$500 \leq Re < 1000$	0.5	0.72	0.36
$1000 \leq Re < 2 \times 10^5$	0.6	$0.35 \bullet \left(\frac{(P/D)_T}{(P/D)_L}\right)^{0.2}$	0.36
$2 \times 10^5 \leq Re < 2 \times 10^6$	0.8	$0.031 \bullet \left(\frac{(P/D)_T}{(P/D)_L}\right)^{0.2}$	0.36

described. More details can be found in (Mateo Marin, 2017).

The Cartesian core model:

The core is represented by a 3D Cartesian VESSEL (component no. 10 in Fig. 7) to describe the fluid domain and by HEAT STRUCTURES to represent the fuel assemblies. The core bypass is modelled by additional PIPE components. The Cartesian VESSEL is nodalized by a radial matrix of 9 × 9, where each Cartesian dimension corresponds to the one of one fuel assembly pitch. Each channel in the vessel represents a fuel assembly except from those that are not needed to represent the core, which are axially and radially blocked, i.e. they are not part in the simulation. A total of 57 out of 81 channels has coolant flow. Axially, each channel is subdivided in 10 nodes. Those levels account only for the active heat transfer height of the core (2 m), as that is all what is needed to effectively check the heat exchange in the core. Two extra axial levels above and below the fuel assemblies are added to represent the volumes at the core inlet and outlet. For each 3D mesh, of the Cartesian VESSEL, the axial and radial flow areas, hydraulic and heated diameters, etc. are provided to TRACE. The SMART fuel assembly is equipped with four spacer grids spread along the active core height. The effect of the spacer grids is considered in the TRACE model as pressure loss represented by a K-factor added axially at the location of each spacer grid, see Sanchez et al (Sanchez-Espinoza et al., 2018). and USNRC (U.S. Nuclear Regulatory Commission, 2012). After the flow area and hydraulic diameter of the channels have been set for vertical and horizontal directions, the fuel assemblies and their connection with the fluid domain must is considered. Each of the 57 HEAT STRUCTURE are represented by TRACE with the same axial levels as the corresponding axial channels of the Cartesian Vessel. The core power is represented by the TRACE POWER component, where more details as the axial and radial power distribution inside the core and the fuel assemblies are defined.

2.5. The integrated reactor pressure vessel (RPV) model

The Integrated RPV of SMART includes the RPV, the core bypass, the pumps, the helical steam generators, and the pressurizer, see Fig. 7. This model is merged with the Cartesian core model described before. It is connected with the containment model corresponding to the first four axial levels of it. The eight helical steam generators are located around the core (component numbers 20 to 27, Fig. 7). They are located in the fourth ring of the VESSEL component (number 100). The pressurizer is located at the top of the RPV and it is presented by a PIPE TRACE component with the type PRESSURIZER (component 80). In addition, it is connected with the IWRST and the safety valves (PORV and SRV). The four canned pumps located over the core are modelled in TRACE (number 41, 42, 43 and 44). Note that the coolant takes a 90° turn during its pass through the canned pumps, the pumps are modelled in such a way to take the coolant from a positive radial direction and inject it at a negative axial direction at axial level 20. In order to model the coolant turn, the second pump cell has a vertical orientation. K-factors are included for the turn and the edges with a change in flow area as predicted in (Sanchez-Espinoza et al., 2018).

The SMART secondary side is represented by the steam lines and header, the feedwater lines, and the passive residual heat removal system (PRHRS). At the inlet and outlet of the helical steam generator coil, a valve is connected (K-factor of 2.78, open during normal operation). This valve connects the PRHRS-pipes with an angle of 90°. The steam header consists of a pipe with 10 nodes where the flow area is growing in the first three nodes until the area of the pipe is equal to the total flow area of all helical coils. All helical coils are connected to the first node of the steam header for better simulation results. The chosen progressive grow in flow area is done based on the experience simulating PWR and its length is approximated so the steam stays under superheated conditions until the BREAK, which simulates the turbine with a pressure of 5.2 MPa.

3. Discussion of selected results

The simulations were performed for standard operation conditions at a core power of 330 MW and for individual assembly powers previously

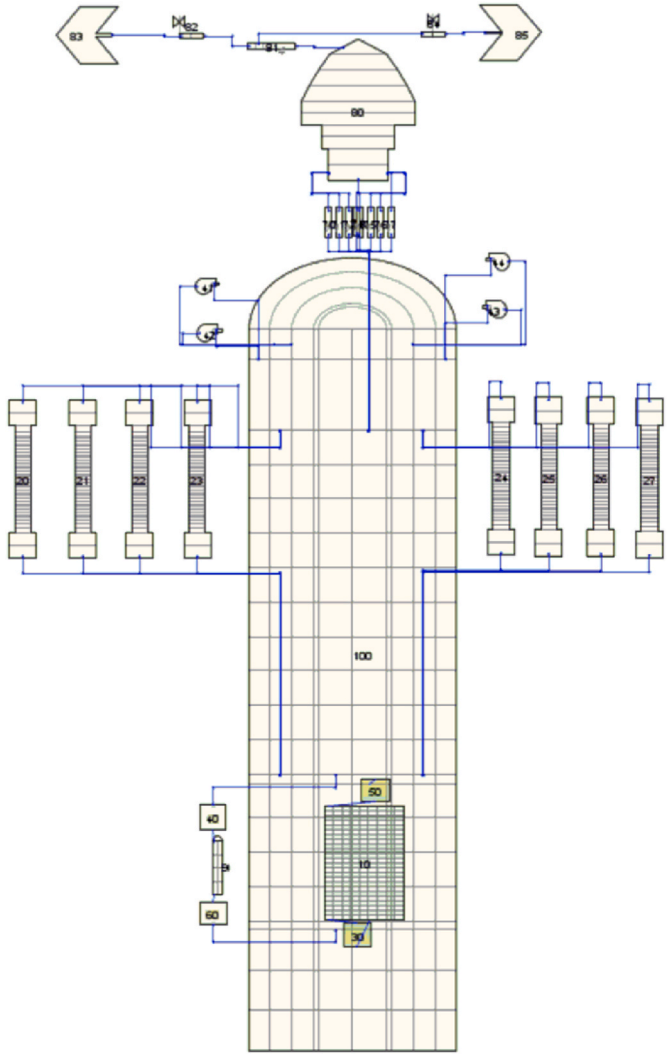

Fig. 7. The integral TRACE model of the SMART integrated reactor consisting of a Cartesian VESSEL (core) and a Cylindrical VESSEL (RPV) and other in-vessel components.

presented in Fig. 5. At a total mass flow of 2090 kg/s and an operating pressure of 15 MPa, while the average core inlet temperature is expected to be 569.2 K. At the core outlet, the coolant is heated up in average by 27 K–596.2 K. Table 3 gives a selection of basic design parameters. Blue colored parameters indicate secondary loop parameters used only by the TRACE model.

In principle an implementation of the water/steam flow of the SG secondary side in the CFD model is possible, but because of convergence problems, an exorbitant increase of computational costs and limited time the authors resigned a further model extension. In Fig. 8, the velocity and coolant temperature distributions calculated by the CFD model are presented. The highest velocities occur at the pump inlets. Because of the large gradients, this model region was most challenging. In addition, large temperature differences and flow separation regions characterize the previously discussed conical gap region that connects the pump inlets with the volume above the active core -formed in its center by control rod guide tube structures. As consequence, the shape could be optimized and technical actions for enhanced mixing in the core region (and above) should be taken into account for further design improvements.

Table 3
SMART main thermal hydraulic parameters.

Total core thermal power	330 MW
Electrical power	100 MW
Operating pressure	17 MPa
Steam pressure	5.2 MPa
Core inlet temperature	569.15 K
Core outlet temperature	596.15 K
Total mass flow	2090 kg/s
Core bypass flow rate	4%
Core inlet velocity	2.1 m/s
Core pressure difference	35 KPa
SG cassette pressure diff.	95 KPa
SG coil pressure loss	180 KPa
Steam mass flow	161 kg/s

The function of the flow skirt and mixer in the lower plenum is to generate a homogeneous mass flow distribution at the core inlet. Fig. 9 presents a comparison of the assembly wise mass flow distribution at the core inlet. The local mass flow for each assembly differs significantly dependent on the radial location from about 38 kg/s in a central location to 29 kg/s in radial outer location. The TRACE simulation predicts the mass flow distribution at the core inlet as significantly more homogeneous because of a much coarser computational mesh and higher numerical diffusion. Concerning the temperature distribution at the core inlet the CFD model predicts differences 567.9 K up to 568.6 K with an average of 568.3 K, which is 0.7 K below the design value. The average temperature at the outlet is predicted as 595.9 K and is only slightly below the expectations. Fig. 10 presents a comparison of cladding temperatures at the contact zone with coolant between CFD and TRACE analysis. Three assorted assemblies were analyzed: the central core position C29 (green color, see also Fig. 5), position B6 (red color) at three layers distance to the center and at a peripheral position A1 (black line) along the core axis. The TRACE values are cross sectional averaged because of the coarse meshing, while the CFD data is extracted along the axial assembly centerlines.

Fig. 10 shows a similar comparison for the maximum fuel temperatures in the center of the fuel rods. The local maxima of all curves agree well with region of locally highest fuel heat release given by the assemblies axial power distribution (Fig. 5, right). While for the central assemblies B and C the local position of the maximum fuel temperature is nearly the same for both cases, the temperature maxima for assembly A shows a small displacement between CFD and TRACE analysis.

A reason therefore may be the consideration of axial heat transfer by conduction in the fuel pins, which is missing in the CFD model. For the cladding material the situation is the same, but obviously to small thickness of this layer of only 0.65 mm the conduction in axial direction is negligible.

For the peripheral assembly A1 we have obviously a very good agreement between CFD and TRACE, but we have to keep in mind that the heat release for A1 (2.5 MW) is the lowest of the presented assemblies (B6: 6.3 MW; C29 8.6 MW). The main impact on the deviations of the cladding temperatures has the difference of the mass flow distribution at the core inlet. For the central assembly C29 the mass flow by CFD is significantly higher because TRACE calculates a significantly homogeneous mass flow and velocity distribution. A higher mass flow leads to improved heat transfer conditions and in consequence up to 10 K lower cladding temperatures. For B6 the situation has changed and mass flow predicted by CFD is lower that leads up to 5 K higher temperatures.

The differences for fuel temperature calculations are locally significantly higher ($\leq$100 K) especially in locations close to the axial top and bottom of the active core zone, see Fig. 11. Several reasons for the deviations can be specified. The TRACE model consists of three radial layers for the fuel zone, one layer for the gap between fuel and cladding and three layers for the cladding. The CFD model is much coarser by consideration of only one layer for each zone. Furthermore, axial conduction cannot be considered in the CFD model. The calculation of fuel temperature is sensitive to the thermal conductivity of UO_2, which has a strong temperature dependency. Because of the low thermal conductivity of UO_2, the fuel region has large temperature differences. As

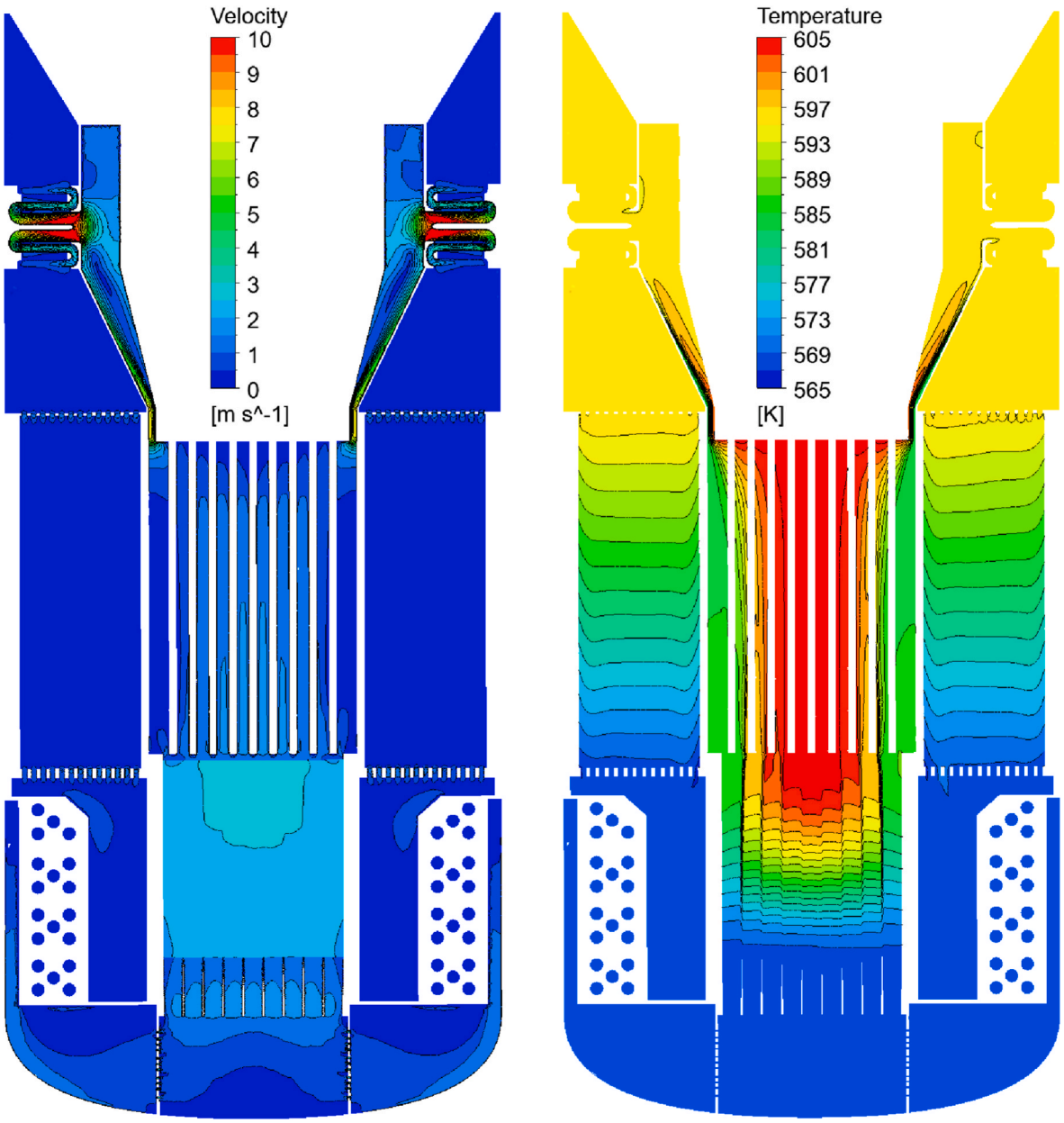

Fig. 8. Velocity and coolant temperature distribution predicted by ANSYS CFX.

consequence, the one layer model for the fuel region by CFD leads to deviations against TRACE. The CFD model has its advantages in modelling the mass and momentum transfer because of the significant better spatial resolution, while TRACE has a more reliable model for the fuel pins.

Finally, SG cladding temperatures on the primary side are compared, see Fig. 12.

While the temperature profile by the CFX model shows a nearly linear decrease from the upper SG inlet to the lower outlet, Trace predicts a stepwise decrease with different gradients. This deviations reflect the different model assumptions. In the CFX model the SG heat sink is assumed as spatially constant, while Trace also models the secondary flow inside the helical coiled SG pipes in counter-flow arrangement. The different gradients of the Trace distribution are caused by multiple flow regimes inside the tubes from liquid at the lower entrance to multiphase flow with increasing void fraction until superheated steam at the outlet.

The influence of different SG heat transfer modelling is mainly limited on the SG Volume if the average temperature at the SG outlet remains the same. Therefore, a more detailed simulation of the secondary flow within the CFD model, which would lead to a significant increase of computational costs in combination with deteriorated numerical stability, is not mandatory.

4. Summary and outlook

In this paper, a CFD model for a small-scaled nuclear pressurized water reactor was presented, where the whole reactor pressure vessel with all internal components was considered as a closed system in the CFD-model. With some extensions, the CFD model was enabled to calculate local core parameters e.g. cladding and fuel temperatures. A qualitative good agreement was obtaining by comparing the CFD results with the one of TRACE considering the different model approaches. The CFD model will provide reference solutions for 1D thermal system codes. Moreover, part of the CFD model will be used for multiscale coupling with TRACE in order to analyze steam line break and ATWS accidents.

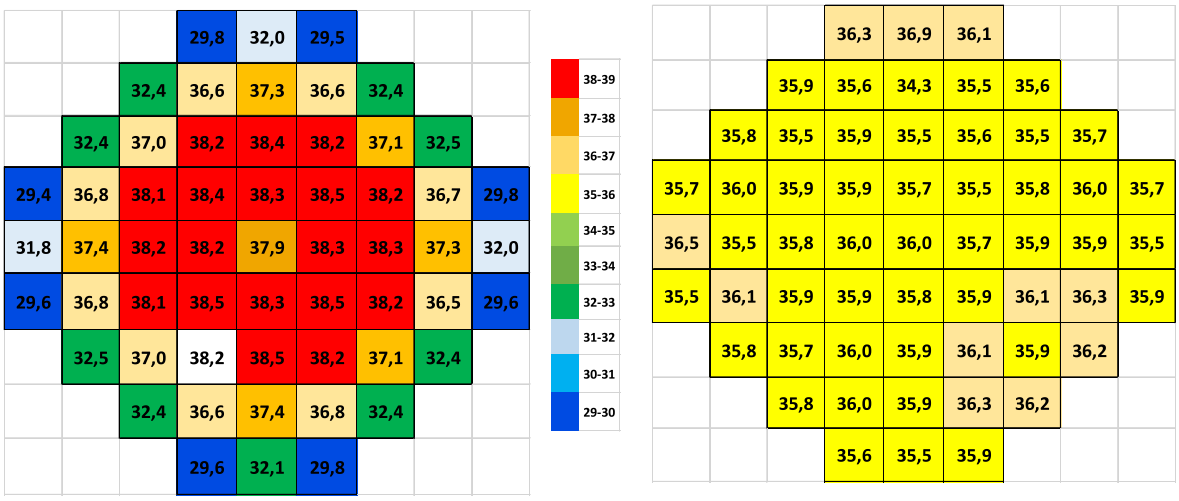

Fig. 9. Assembly mass flow distribution in kg/s at the core inlet for CFD (left) and TRACE simulation (right).

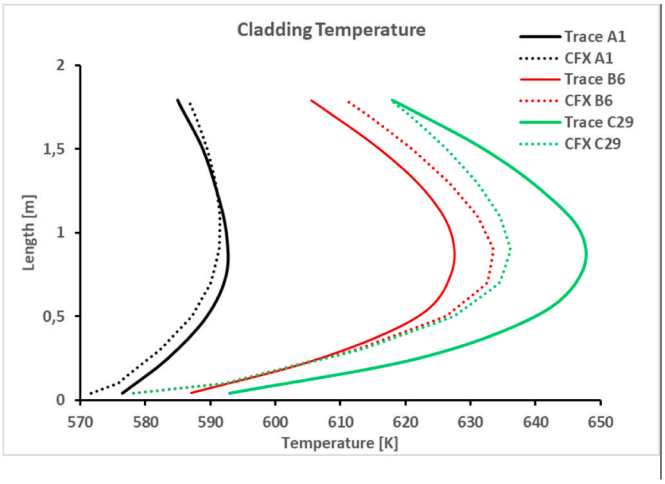

Fig. 10. Comparison of the axial cladding temperature predicted by CFX and TRACE.

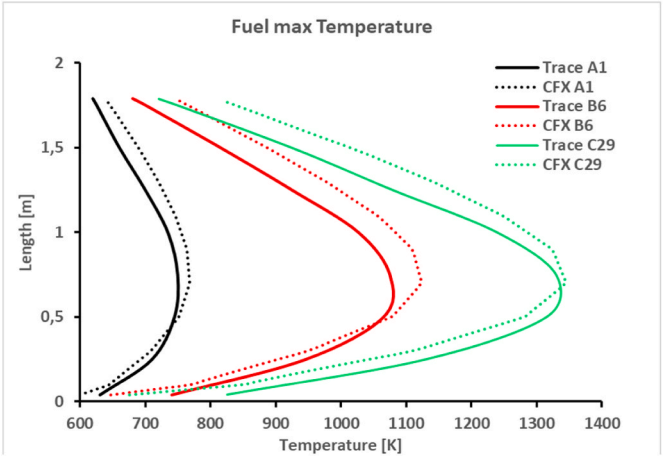

Fig. 11. Comparison of the maximal fuel temperature in the core.

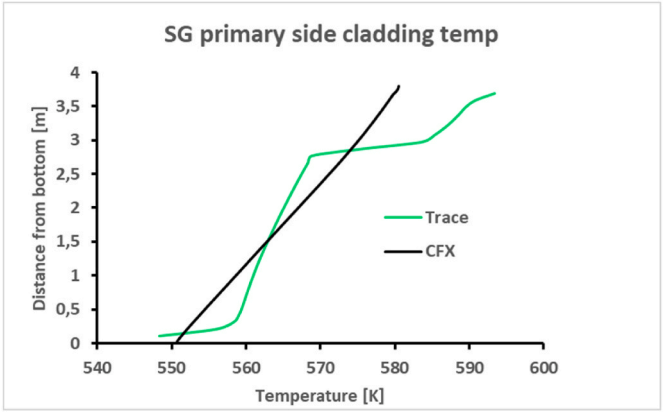

Fig. 12. Comparison of SG rod temperatures at primary side.

Declaration of competing interest

The authors declare that they have no known competing financial interests or personal relationships that could have appeared to influence the work reported in this paper.

Data availability

The authors do not have permission to share data.

Acknowledgments

This work has received funding from the Euratom research and training program 2019–2020 under grant agreement No 945063 H2020 McSAFER project and the NUSAFE program of the Karlsruhe Institute of Technology (KIT).

List of Abbreviations and Acronyms

ATWS	Anticipated Transient Without SCRAM
CAD	Computer Aided Design
CFD	Computational Fluid Dynamics
IWRST	In-containment Refueling Water Storage Tank
KAERI	Korea Atomic Energy Research Institute
PORV	Pressure-Operated Relief Valves
PRHRS	Passive Residual Heat Removal Systems
SRV	Safety Relief Valves

SG	Steam Generator
SMR	Small Modular Reactor
SMART	**S**ystem integrated **M**odular **A**dvanced **R**eac**T**ors
TRACE	Trace/Relap Advanced Computational Engine
VVER	Water-Water-Energy Reactor

References

Bae, Y., Kim, Y.I., Park, a.C.T., 2013. CFD analysis of flow distribution at the core inlet of SMART. Nucl. Eng. Des. 258, 19–25.

Böttcher, M., Krüßmann, R., 2010. Primary loop study of a VVER-1000 reactor with special focus on coolant mixing. Nucl. Eng. Des. 240, 2244–2253, 2244–2253, 240 February 2010.

Choi, S., 2014. Small modular reactors (SMRs): the case of the Republic of Korea. In: Handbook of Small Modular Reactors. Elsevier, pp. 379–407.

Filonenko, G.K., 1954. Hydraulic Resistance in Pipes. Teplonergetika, pp. 40–44.

Gnielinski, V., 1976. New equations flow regime heat and mass transfer in turbulent pipe and channel flow. Int. Chem. Eng. 16, 359–368.

Horelik, N., Herman, B., Forget, B., Smith, a.K., 2013. Benchmark for evaluation and validation of reactor simulations (BEAVRS), v1.0.1. In: Proc. Int. Conf. Mathematics and Computational Methods Applied to Nuclear Science and Engineering. Sun Valley, Idaho.

IAEA, 2005. Optimization of the Coupling of Nuclear Reactors and Desalination Systems. IAEA, Viena.

Kim, S., El-Genk, M., 1988. “Heat transfer experiments for low flow of water in rod bundles“. Int. J. Heat Mass Tran. 32 (7), 1321–1336.

Kim, Y., Bae, Y., Chung, Y., 2015. K. & Kim, "CFD Simulation of Thermal Mixing in Flow Mixing Header Assemby of SMART". International Symposium on Turbulence and Shear Flow, Melbourne.

Kolev, N., Petrov, N., Donov, J., Angelova, D., Aniel, S., Royer, .E., Ivanov, K., Lukanov, E., Dinkov, Y., Popov, D., Nikonov, S., 2006. VVER-1000 Coolant Transient Benchmark – Phase 2 (V1000CT-2). Vol. Ll: MSLB Problem – Final Specifications., vol. 6. NEA/NSC/DOC.

Mateo Marin, V., 2017. Development of an Integral Thermal-Hydraulic Plant Model for a Small Modular Reactor (Smart) Using the Best-Estimatecode System Trace. UPM. Master Thesis, Madrid. Spain.

Menter, F.R., 1993. Zonal Two Equation K-ω Turbulence Models for Aerodynamic Flows. AIAA, pp. 93–2906.

Sanchez-Espinoza, V., Marin, V.M., Alzaben, Y., Jimenez, G., Stieglitz, a.R., 2018. " integral SMART plant model development using the system thermal-hydraulic code TRACE for transient analysis,". In: The 12th International Topical Meeting on Nuclear Reactor Thermal Hydraulics, Operation and Safety. Qingdao, China, October 14-18.

Sanchez-Espinoza, V.H., Gabriel, S., Suikkanen, H., Telkkä, J., Valtavirta, V., Bencik, M., Kliem, S., Queral, C., Farda, A., Abéguilé, F., Smith, P., Uffelen, P.V., Ammirabile, L., Seidl, M., Schneidesch, C., Grishchenko, D., Lestani, H., 2021. The H2020 McSAFER project: main goals, technical work, program, and status. Energies 6348, 14.

TRACE 5.0 Patch 6 Theory Manual, 2013. U. S. Nuclear Regulatory Commission, Washington, DC 20555-0001.

U.S. Nuclear Regulatory Commission, 2012. TRACE Pressurized Water Reactor Modelling Guidance.

Wang, Mingjun, et al., 2020a. CFD simulation on the flow characteristics in the PWR lower plenum with different internal structures. Nucl. Eng. Des. 364, 110705.

Wang, Lianfa, et al., 2020b. Numerical simulation of temperature heterogeneity inside the AP1000 upper plenum and hot leg. Nucl. Eng. Des. 362C, 110525.

Wang, Mingjun, Manera, Annalisa, Petrov, Victor, et al., 2020c. Passive decay heat removal (DHR) system design for the integral inherent safety light water reactor (I2S-LWR) [J]. Ann. Nucl. Energy 145, 106987.

Wang, Mingjun, et al., 2021. Recent progress of CFD applications in PWR thermal hydraulics study and future directions. Ann. Nucl. Energy 150, 107836.